Theoretical study of two-dimensional pentamode metamaterials with arbitrary primitive cells

Q. LI[*,1,2], K. WU[1], M. ZHANG[1]
[1]*Naval Architecture and Ocean Engineering College, Dalian Maritime University, Dalian, 116026, China*
[2]*Polar Shipping and Safety Institute, Dalian Maritime University, Dalian, 116026, China*

Pentamode metamaterials are those with vanishing shear modulus that can only resist compressional stresses. In this paper, two-dimensional pentamode metamaterials with arbitrary primitive cell are studied. The phononic band structures of selected primitive cells are calculated to verify that there are pentamode bands where only compressional waves exist. The band widths of different unit cells are calculated to show the effect of the cell shape on the pentamode bands. The effect of geometric parameters of the primitive cells on their effective properties are also analyzed. Acoustic waves in water with pentamode cells are simulated to show the water-like properties.

(Received March 4, 2022; accepted August 10, 2022)

Keywords: Acoustic metamaterials, Pentamode metamaterials, Arbitrary primitive cell, Phononic band structures

1. Introduction

Acoustic metamaterials [1] are artificial materials that can manipulate and control acoustic waves with characteristics that may be impossible for conventional materials. With the interesting properties, acoustic metamaterials have been receiving more and more attention.

Pentamode metamaterial (PM) is one kind of acoustic metamaterials. Bimode and PMs were presented by Milton and Cherkaev [2] in 1995. Bimode metamaterials are also called PMs because they are the two-dimensional (2D) equivalent to three-dimensional (3D) PMs. They have solid structures but possess properties similar to liquids. They have finite bulk modulus and vanishing shear modulus. Therefore, they are also named 'metafluid' [3].

More and more researchers have focused on the novel materials after Norris [4] proposed that they could be used for acoustic cloaking. Kadic et al. [5] proved the practicability of the PMs of face-centered-cubic unit cell by calculating the ratio of bulk modulus to shear modulus. The phononic band structures [6] of the unit cells were also calculated to show the shear mode band gaps. Anisotropic properties of the unit cells were derived by changing their structure parameters [7]. The effective properties of the PMs were tailored by varying structural parameters [8, 9]. PMs with other unit cells [10-12] or with different arm cross-sections [13] or with asymmetric double-cone elements [14] or with core-shell structures [15] were proposed. PMs with composite structures [16-18] were also studied numerically.

Compared with 3D PMs, 2D models also have similar properties but are easier to fabricate. 2D models were also studied numerically and experimentally in the past years. The effective properties of hexagonal PMs were studied for different parameters [19]. The properties were experimentally verified [20-21]. Effective properties and potential applications of a highly anisotropic pentamode element were analyzed [22]. Multiphase unit cells [23] were also studied which have more parameters to affect the effective properties. The PMs have high potential in various acoustic wave controlling situations. The 2D PMs were used for focusing underwater sound [24], manipulating wavefronts [25-27], bending waves [3] and multiplexing communication [28]. They were also used in 2D carpet cloak [29] and omnidirectional cloak [30, 31].

Although PMs have been studied for several years, little research is found on arbitrary 2D unit cells. In this paper, 2D PMs with arbitrary primitive cells were studied theoretically. Any area of parallelogram can be filled with PM unit cells with uniform boundaries, and there are more degrees-of-freedom to tailor the effective properties of 2D PMs. The phononic band structures of primitive cells were calculated within the irreducible Brillouin zone (IBZ). PM band width of different primitive cells were calculated. The anisotropy and effective properties of the models with variation of geometric parameters were analyzed. Acoustic waves in water with and without PMs were simulated.

2. Modeling

The 2D unit cells are parallelograms which take five

different Bravais lattices, namely oblique, rectangular, centered rectangular, square and hexagonal [32]. The traditional unit cells adopted in 2D PMs are usually hexagonal ones. In order to design a general model of 2D PMs, a primitive cell of parallelogram is used, as shown in Fig. 1. When wavelength is much larger than the unit cell dimensions, the materials can be homogenized with effective properties. The length of AB, set as length unit, is held fixed throughout the paper, and noted as l. Arbitrary primitive cell in 2D can be derived by changing the parameters of α and β. Especially, when $\alpha = \beta = 30°$, it is hexagonal; when $\alpha = \beta = 45°$, it is square; when $\alpha \neq \beta$ and $\alpha + \beta = 90°$, it is rectangular; when $\alpha = \beta \neq 45°$, it is rhombic.

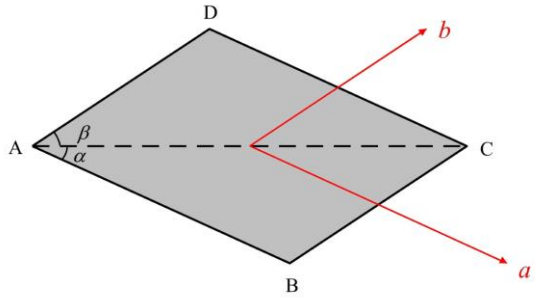

Fig. 1. General model of a two-dimensional primitive cell

The structures of the primitive cell are composed of diamond arms with rectangular ends at the tips, as shown in Fig. 2. The dimensions of the arm are denoted by d_1 (the width of the rectangle) and d_2 (the width of the middle of the diamond). Three arms are connected at point P. The position of P can be controlled by

$$\overrightarrow{AP} = \eta_1 \overrightarrow{AB} + \eta_2 \overrightarrow{AD} \ ,$$

where η_1, η_2 are coefficients.

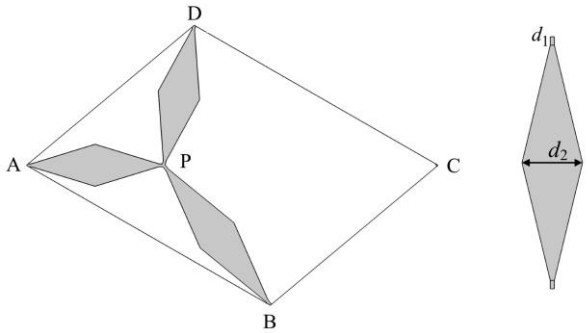

Fig. 2. Primitive cell of general two-dimensional pentamode matematerials

The properties of the primitive cells can be derived from their first Brillouin zone. The first Brillouin zones are rectangles, squares or hexagons. The first Brillouin zone of two specific models are shown in Fig. 3. Fig. 3(a) shows the first Brillouin zone of an oblique cell with α = 30° and β = 40°, while Fig. 3(b) shows the first Brillouin zone of a rectangular unit cell with α = 50° and β = 40°. They are both centrosymmetric.

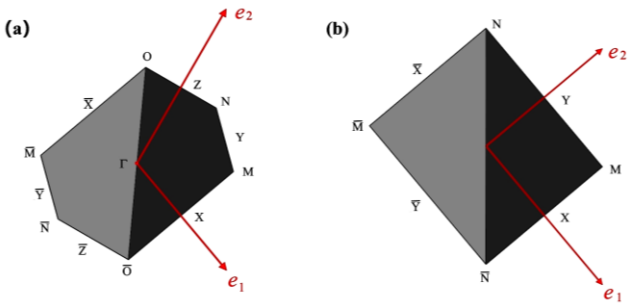

Fig. 3. The first Brillouin zone of the primitive cells (a) α = 30°, β = 40° (b) α = 50°, β = 40°

The band structures are calculated with finite element software COMSOL Multiphysics®. The Cauchy Momentum Equation is used to solve the eigenfrequencies of the cells, which is

$$-\rho\omega^2\mathbf{u} = \nabla \cdot \boldsymbol{\sigma}$$

where ρ is density, $\mathbf{u}$ is the displacement vector, and $\boldsymbol{\sigma}$ is the stress tensor.

The boundary conditions were set as floquet periodic. The material of the arms was set with aluminum (E = 76 GPa, ρ = 2700 kg/m^3, Poisson's ratio = 0.33). Band structures of hexagonal unit cells are usually calculated around their irreducible Brillouin zone (IBZ) contours. However, there exist probabilities that band gap extremum may locate within the zones instead of the contours for non-symmetric unit cells [33]. The phononic bands for half the zone of the IBZ were calculated for accurate results. The band structures of the oblique model (α = 30°, β = 40°) and the rectangular model (α = 50°, β = 40°) are calculated within the darker area in Fig. 3. The other parameters are d_1=0.01l, d_2=0.15l, η_1 = 1/3 and η_2 = 1/3. In this paper, l=0.01m for all the cells. Each band is calculated from the center to the boundary every 0.02 rad. The bands are shown in Fig. 4(a) and Fig. 4(c). There are bands where only compressional wave exists. The pentamode band can be obtained by mapping the 3D bands to 2D, as shown in Fig. 4(b) and Fig. 4(d).

It can also be seen from Fig. 4 that the pentamode bands are different for different unit cells even with the same arm dimensions. The band limits for aluminum primitive cells with d_1=0.01l, d_2=0.15l, and η_1= η_2 =1/3 are calculated for different α and β. The results are shown in Fig. 5. It shows that the bands vary greatly with α and β. The width of the pentamode band decreases with the increase of α and β from the trend of the figure. Smaller values of α and β are preferred if wide pentamode bands are desired. Pentamode bands disappear when the maximum angle of the primitive cell is too large.

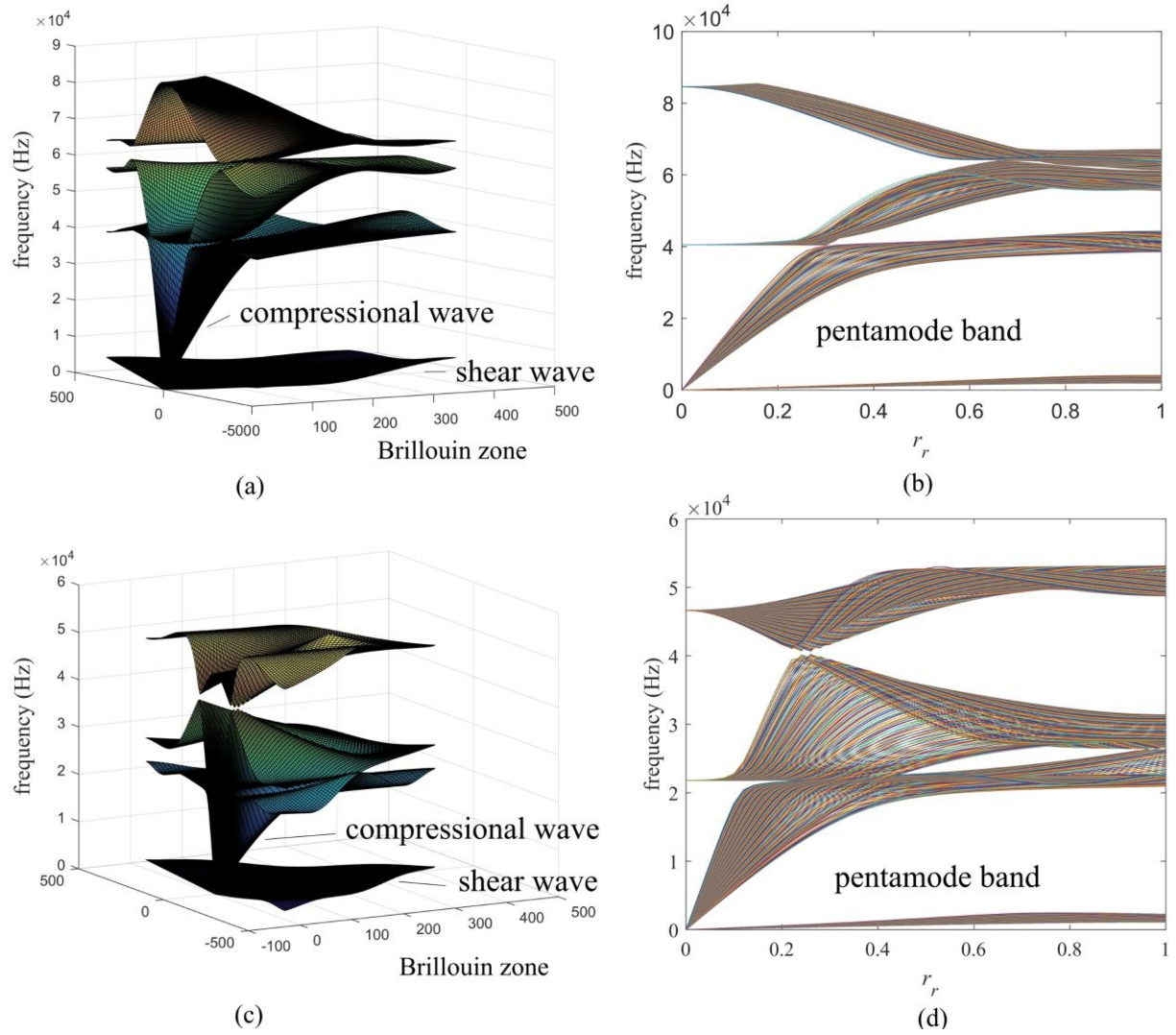

Fig. 4. The band structures of the pentamode models: (a) 3D and (b) 2D band for oblique primitive cell with $\alpha = 30°$, $\beta = 40°$; (c) 3D and (d) 2D band for rectangular primitive cell with $\alpha = 50°$, $\beta = 40°$ (color online)

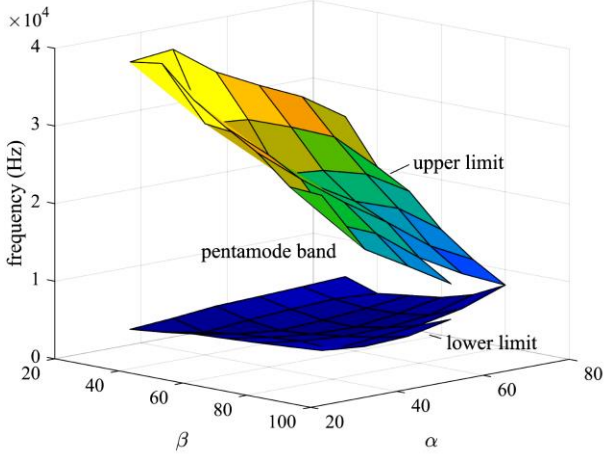

Fig. 5. Pentamode band limits for primitive cells with $d_1=0.01l$, $d_2=0.15l$, and $\eta_1 = \eta_2 = 1/3$ (color online)

3. Properties

The geometric parameters play an important role in changing its properties besides the pentamode band width. The slope of the band branch starting from the center is the velocity along that direction. The extremum of the compressional wave and shear wave velocities for aluminum unit cells with $d_1=0.01l$, $d_2=0.15l$, $\eta_1 = \eta_2 = 1/3$ are calculated for primitive cells with different β. The results are shown in Fig. 6. The angle α is 30° in Fig. 6(a). Isotropy is obtained when $\alpha = \beta = 30°$. Otherwise, the primitive cells are anisotropic. Anisotropy increases when β deviates from 30°. There is no isotropic cell when $\alpha = 60°$, as shown in Fig. 6(b). High anisotropy of compressional wave velocities as much as 60 can be derived when $\alpha = 60°$ and $\beta = 100°$. However, the lowest compressional wave velocity is comparable with shear wave velocities when anisotropy is high.

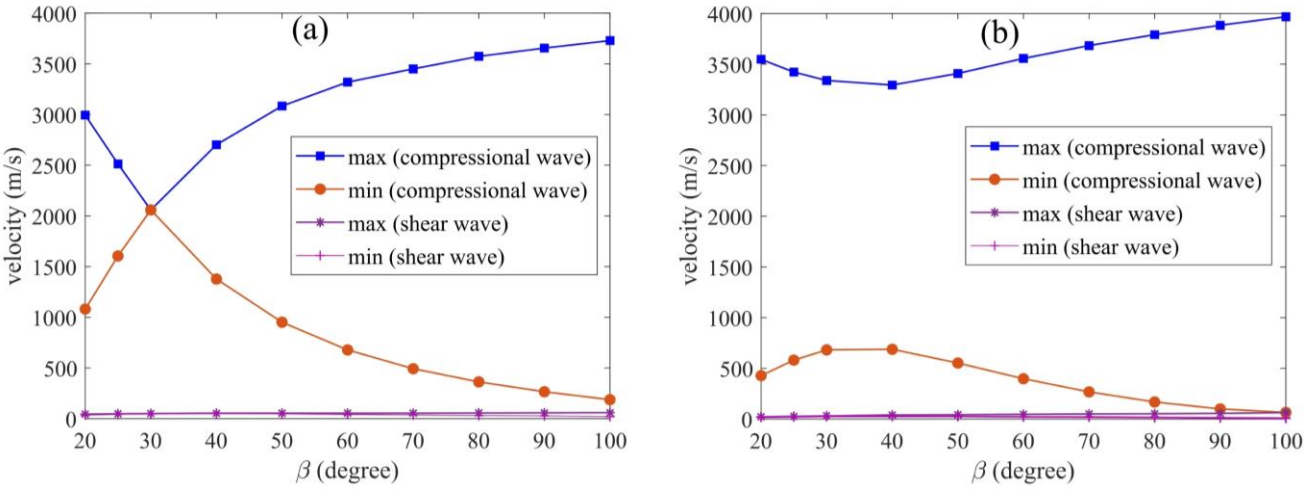

Fig. 6. Maximum and minimum of compressional wave and shear wave velocities for primitive cells with (a) $\alpha = 30°$ (b) $\alpha = 60°$ (color online)

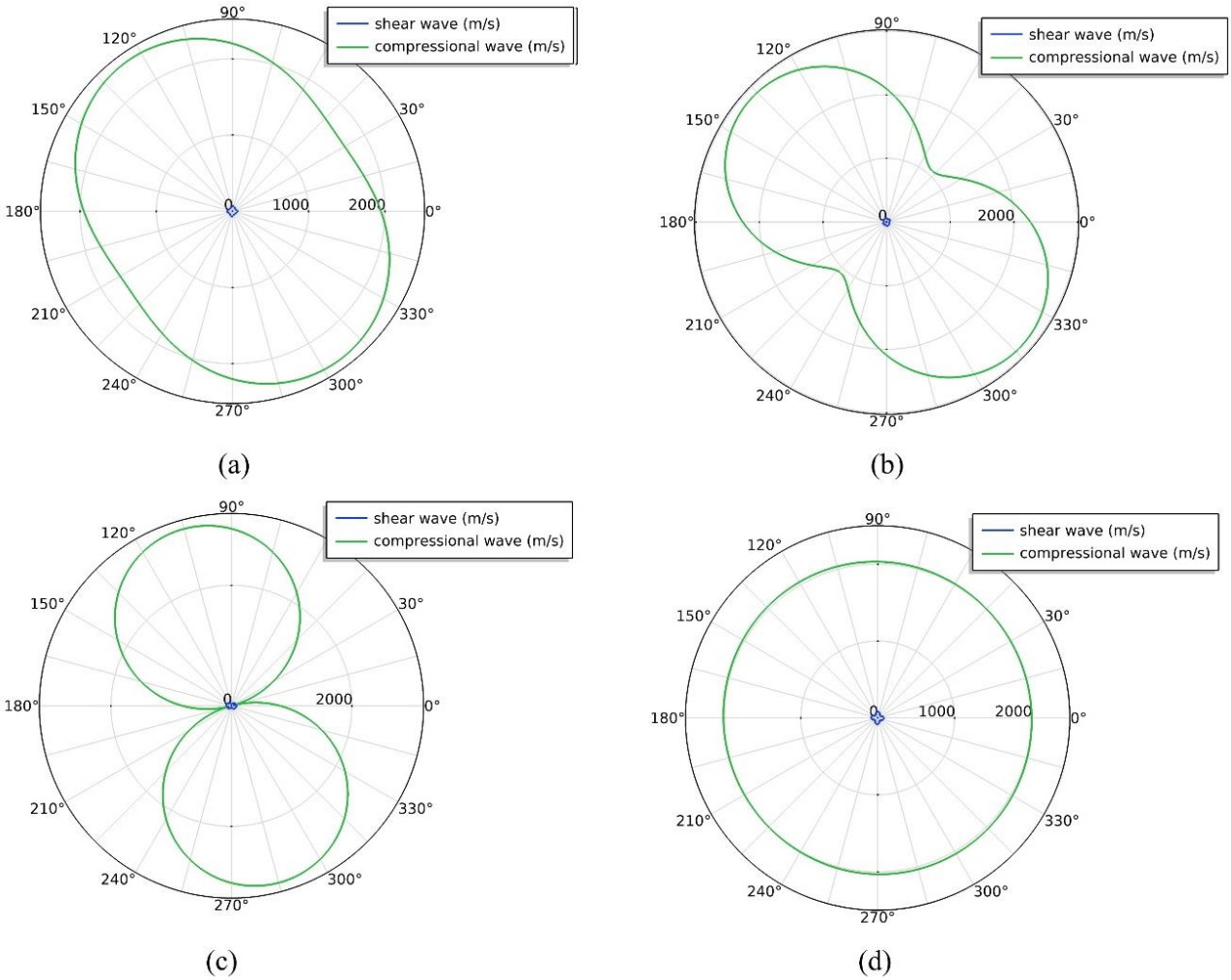

Fig. 7. The velocities along different directions for oblique models with (a) $\eta_1 = 0.24$, $\eta_2 = 0.36$ (b) $\eta_1 = 0.40$, $\eta_2 = 0.20$ (c) $\eta_1 = 0.5$, $\eta_2 = 0.5$ (d) $\eta_1 = 0.17$, $\eta_2 = 0.37$ (color online)

Besides the dimensions of the primitive cell, the parameters within the primitive cell also affect the effective properties. The position of point P can be varied within the primitive cell. The effective velocities of the oblique cell (α = 30°, β = 40°) along different directions are calculated with variation of the connection point P. The results of 4 cases are shown in Fig. 7. The dimensions of the arm are $d_1 = 0.01l$ and $d_2 = 0.15l$, and the material is aluminum. It can be seen from the figures that the shear wave velocities are negligible compared with those of the compressional waves and the anisotropy can be tailored significantly by η_1 and η_2. High anisotropy as much as 30 is derived with maximum velocity higher than 3000 m/s and minimum velocity lower than 100 m/s, as shown in Fig. 7(c). Also, isotropy can also be derived by varying the parameters. The primitive cell is quasi-isotropic with η_1 = 0.17 and η_2 = 0.37, as shown in Fig. 7(d). It needs to be noted that the effect of η_1 and η_2 on different primitive cells are not the same. The anisotropy and the directions of the maximum velocities are different for different primitive cells even with the same η_1 and η_2.

The dimensions of the arms on the effective properties are also studied. The oblique cell (α = 30°, β = 40°) is taken as an example. Aluminum is chosen as materials for the arms. The position of the connection point is set as $\eta_1 = \eta_2 = 1/3$. The effects of d_1 and d_2 on the compressional wave velocities are studied, as shown in Fig. 8. It shows that both the minimum and the maximum of the compressional wave velocities increase with d_1 and decrease with d_2. Same phenomena were found for other primitive cells. It can be explained that the parameter d_1 mainly affects the effective stiffness and the parameter d_2 mainly affects the effective density. The geometric parameters of the arms also play an important role in affecting the effective properties. It can be drawn that the combination of all the geometric parameters affect the effective properties. That also means the effective properties can be tailored by the parameters. Since the number of parameters increases with this model, there are more ways to get the unit cell with desired properties.

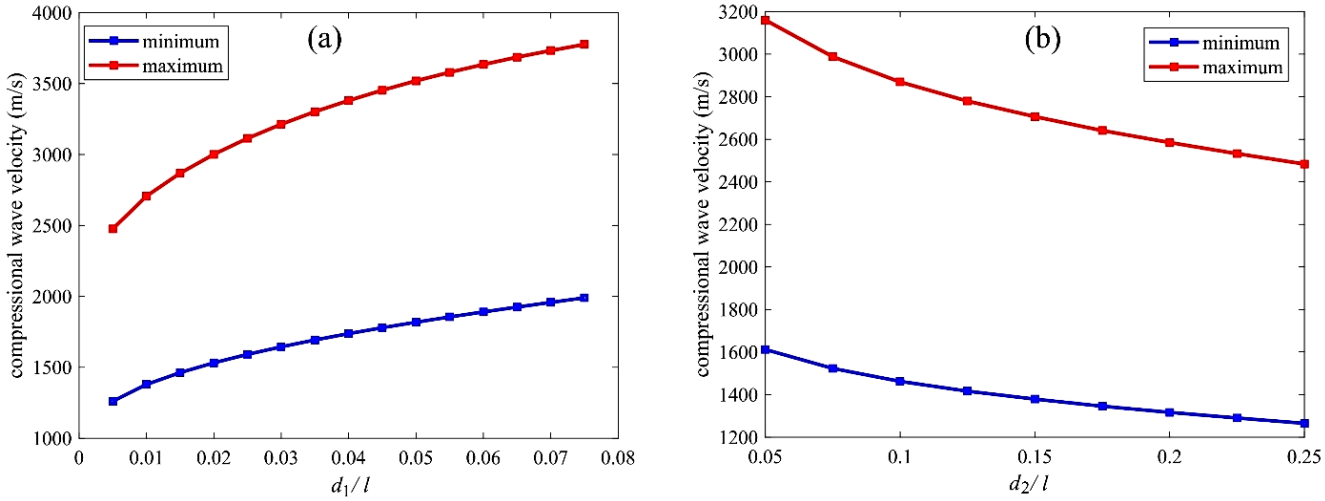

Fig. 8. The variation of compressional wave velocities with dimensional parameters (color online)

4. Simulations

Full-wave simulations were conducted with COMSOL Multiphysics® to verify the effective properties of the PMs. Simulations of an acoustic wave through a water domain with a rectangular area were conducted. Part of the left boundary was set as port and the other boundaries were set as plane wave radiation which allows no reflection.

An oblique unit cell with α = 30° and β = 40° is taken as an example. The band structure along one direction is calculated, as shown in Fig. 9(a). The effective velocity is 1396 m/s and the effective density is 452 kg/m^3. The performance of the unit cells was verified with acoustic waves in water, as shown in Fig. 9(b). There was an area in each field which was the unit cells with water inside or the unit cells with air inside or water, respectively. It can be seen from the results that the PMs with water inside allows the acoustic energy to pass but affects the effective velocity that deviates from the theoretical values. Same conclusion was drawn from simulations with rectangular unit cells. The PMs with air inside show the velocity approximate to the theoretical values but the acoustic energy is weakened compared with the water. The reason is due to the acoustic impedance of the PMs with air inside is not matched with

that of water, and part of the acoustic energy is reflected.

To find a unit cell with acoustic impedance matched with water, copper was used instead of aluminum. A unit cell with effective density 1503 kg/m^3 and effective velocity 1010 m/s was found by adjusting the dimensions. Simulations and performance of PMs with the impedance matched unit cells are shown in Fig. 10. A material with theoretical values was also simulated for comparison. The pressure field with PMs is close to that with a material of the theoretical values. They have a lower velocity than water and the amplitudes seem similar to water. It can be seen from Fig. 10(b) that there are small fluctuations of the sound pressure levels (SPLs) before the PMs, but the SPLs after the PMs follow the trends of the water in different frequencies. They are close to each other at specific frequency ranges.

At lower frequencies where shear waves exist, the amplitudes are weakened. It can be explained by analyzing the modes of the PMs. The modes at 1000 Hz and at 10000 Hz are shown in Fig. 11. It can be seen that shear modes dominate at 1000 Hz and compressional mode dominates at 10000 Hz. The acoustic energy is dissipated by the shear waves at 1000 Hz.

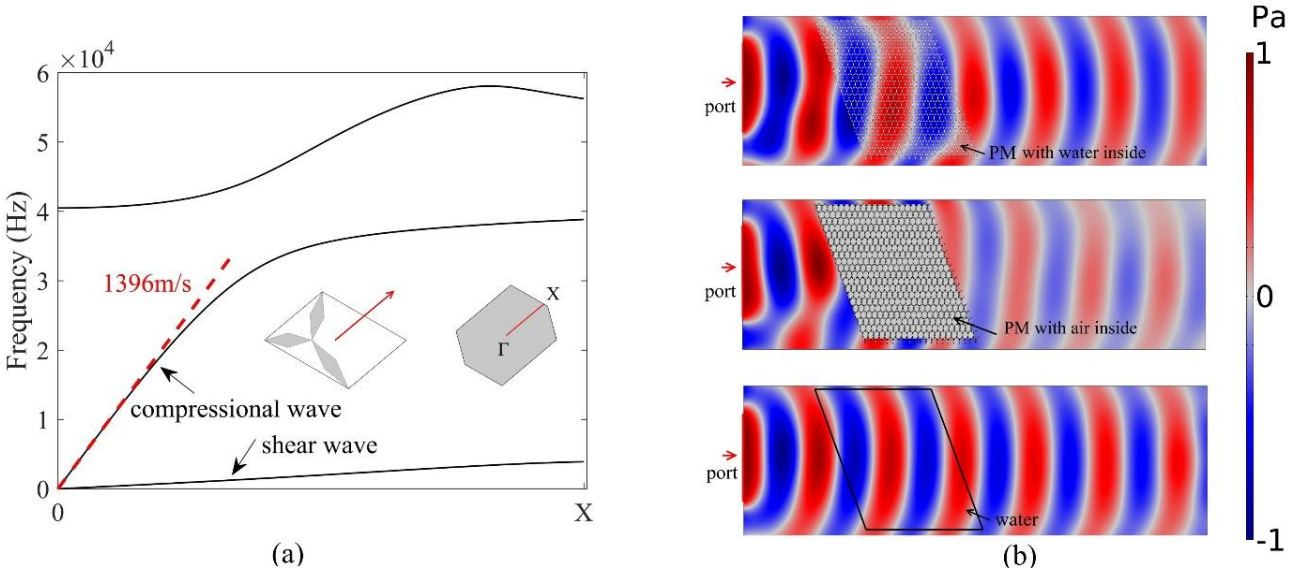

Fig. 9. Band structures of the unit cell along one direction and the acoustic waves through water with and without PMs (a) band structures along one direction (b) simulation of acoustic waves (color online)

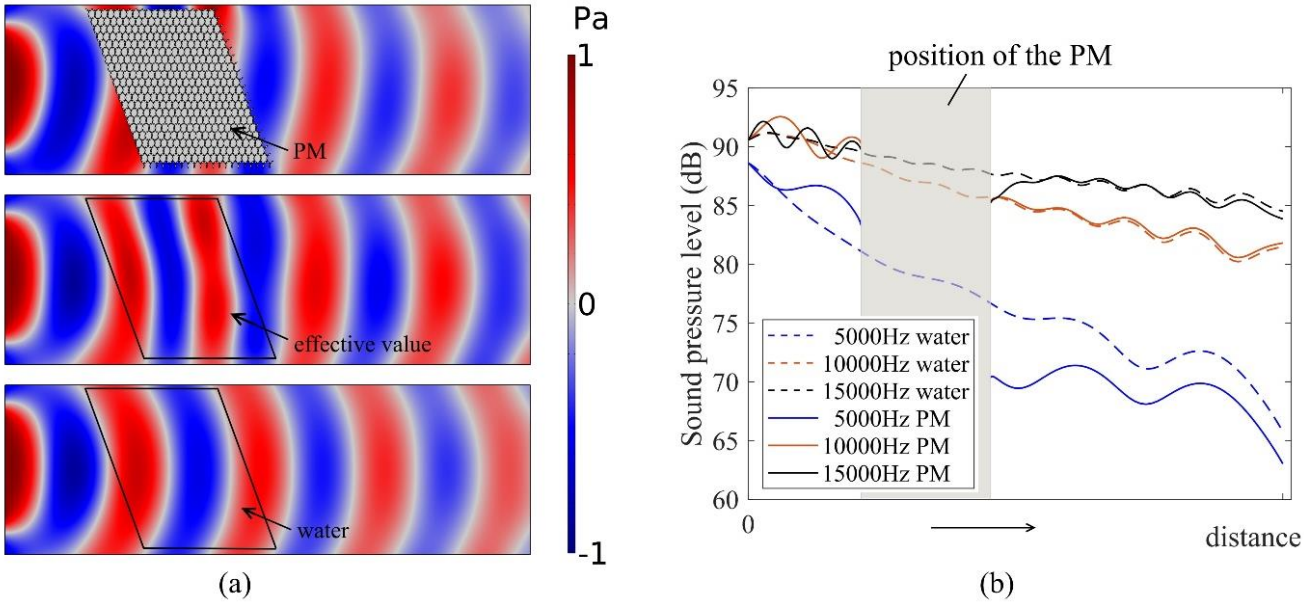

Fig. 10. Simulations and performance of the impedance matched PMs (a) acoustic field with impedance matched PMs, theoretical values and water (b) sound pressure levels along center-lines of the fields with PMs and water (color online)

The results show that the PMs have water-like properties with little energy loss at their PM bands. The effective properties of the PMs are usually comparable with those of water. If the PMs are filled with water, the effective properties of PMs are greatly influenced. The effective velocities are around that of water, and transmission can be guaranteed if proper parameters of the unit cell are selected. If the PMs are filled with air, the effective properties are close to the theoretical values. If acoustic impedance is matched, the transmission is also guaranteed.

The effective properties of the primitive cells can be tailored greatly by the parameters. Thus, they have potential in various applications with strict requirements.

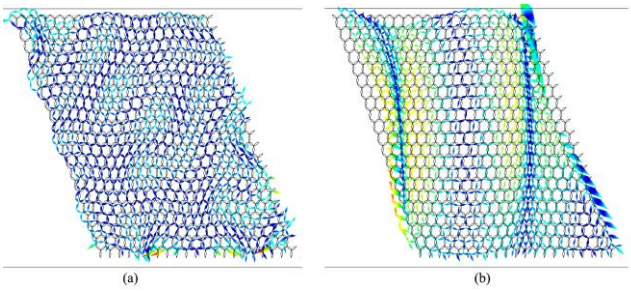

Fig. 11. The modes of PMs at different frequencies (a) 1000 Hz (b) 10000 Hz (color online)

5. Conclusions

In this paper, two-dimensional pentamode metamaterials with arbitrary primitive cells are studied. The model is composed of tri-arm structures. The phononic band structures show that they have pentamode bands where only compressional mode exists. The band width varies with primitive cells. The pentamode bands disappear when the maximum angle of the primitive cell is too large.

The effective velocities can be tailored greatly by the geometric parameters. Anisotropy can be tuned by changing the primitive cell shapes only. Isotropic properties and high anisotropy of 60 in compressional wave velocities can be obtained for specific models. Isotropic properties and high anisotropy of 30 in compressional wave velocities can be obtained by changing the position of the connection point of an oblique cell. The geometric dimensions of the arms also affect the effective properties. The compressional wave velocities increase with the tip dimension and decrease with the middle dimension. All the parameters are combined in affecting the effective properties, leading to the fact there are more degrees-of-freedom to satisfy specific requirements.

If only water-like properties are required, the PMs can be filled with water. But if the effective velocities are also restricted, the PMs should be filled with air. The transmission of acoustic waves is high when acoustic impedance is matched. They have great potential in acoustic applications where strict properties are required.

Acknowledgements

The research was supported by National Natural Science Foundation of China (52001046) and Central University Basic Research Fund of China (3132021112, 3132019308).

References

[1] S. A. Cummer, J. Christensen, A. Alù, Nat. Rev. Mater. **1**, 16001 (2016).
[2] G. W. Milton, A. V. Cherkaev, J. Eng. Mater. Technol. **117**(4), 483 (1995).
[3] Z. Sun, H. Jia, Y. Chen, Z. Wang, J. Yang, J. Acoust. Soc. Am. **143**(2), 1029 (2018).
[4] A. N. Norris, Proc. R. Soc. A **464**(2097), 2411 (2008).
[5] M. Kadic, T. Bückmann, N. Stenger, M. Thiel, M. Wegener, Appl. Phys. Lett. **100**(19), 191901 (2012).
[6] A. Martin, M. Kadic, R. Schittny, T. Bückmann, M. Wegener, Phys. Rev. B **86**(15), 155116 (2012).
[7] M. Kadic, T. Bückmann, R. Schittny, M. Wegener, New J. Phys. **15**(2), 023029 (2013).
[8] M. Kadic, T. Bückmann, R. Schittny, P. Gumbsch, M. Wegener, Phys. Rev. Appl. **2**(5), 054007 (2014).
[9] Z. Wang, C. Cai, Q. Li, J. Li, Z. Xu, J. Appl. Phys. **120**(2), 024903 (2016).
[10] G. Wang, L. Jin, L. Zhang, Z. Xu, AIP Adv. **7**(2), 025309 (2017).
[11] Y. Huang, X. Lu, G. Liang, Z. Xu, J. Appl. Phys. **121**(12), 125110 (2017).
[12] Q. Li, J. S. Vipperman, J. Acoust. Soc. Am. **145**(3), 1372 (2019).
[13] Y. Huang, X. Lu, G. Liang, Z. Xu, Phys. Lett. A **380**(13), 1334 (2016).
[14] C. Cai, Z. Wang, Q. Li, Z. Xu, X. Tian, J. Phys. D: Appl. Phys. **48**(17), 175103 (2015).
[15] Y. Huang, X. Zhang, H. Li, C. Cai, Phys. Scr. **96**(10), 105702 (2021).
[16] Z. Wang, Y. Chu, C. Cai, G. Liu, M. R. Wang, J. Appl. Phys. **122**(2), 025114 (2017).
[17] C. Cai, C. Han, J. Wu, Z. Wang, Q. Zhang, J. Phys. D: Appl. Phys. **52**(4), 045601 (2018).
[18] Q. Li, M. Zhang, J. Phys.- Condens. Matter. **32**(47), 475701 (2020).
[19] X. Cai, L. Wang, Z. Zhao, A. Zhao, X. Zhang, T. Wu, H. Chen, Appl. Phys. Lett. **109**(13), 131904 (2016).
[20] L. Zhang, B. Song, A. Zhao, R. Liu, L. Yang, Y. Shi, Compos. Struct. **226**, 111199 (2019).
[21] A. Zhao, Z. Zhao, X. Zhang, X. Cai, L. Wang, T. Wu, H. Chen, Appl. Phys. Lett. **110**(1), 011907 (2017).

[22] C. N. Layman, C. J. Naify, T. P. Martin, D. C. Calvo, G. J. Orris, Phys. Rev. Lett. **111**(2), 024302 (2013).
[23] A. Zhao, X. Zhang, W. Yu, Z. Zhao, X. Cai, H. Chen, Appl. Phys. Lett. **118**(22), 224103 (2021).
[24] X. Su, A. N. Norris, C. W. Cushing, M. R. Haberman, P. S. Wilson, J. Acoust. Soc. Am. **141**(6), 4408 (2017).
[25] Y. Liu, Y. Li, X. Liu, Chin. Phys. B **28**(2), 024301 (2019).
[26] Y. Tian, Q. Wei, Y. Cheng, Z. Xu, X. Liu, Appl. Phys. Lett. **107**(22), 221906 (2015).
[27] Y. Chu, Z. Wang, Z. Xu, Phys. Lett. A **384**(11), 126230 (2020).
[28] Z. Sun, Y. Shi, X. Sun, H. Jia, Z. Jin, K. Deng, J. Yang, J. Phys. D: Appl. Phys. **54**(20), 205303 (2021).
[29] J. Chen, J. Liu, X. Liu, AIP Adv. **8**(8), 085024 (2018).
[30] Y. Chen, X. Liu, G. Hu, Sci. Rep. **5**, 15745 (2015).
[31] Y. Chen, M. Zheng, X. Liu, Y. Bi, Z. Sun, P. Xiang, J. Yang, G. Hu, Phys. Rev. B **95**(18), 180104 (2017).
[32] C. Kittel, "Introduction to Solid State Physics (eighth edition)", John Willey and Sons, Inc., Hoboken, 6 (2005).
[33] F. Maurin, C. Claeys, E. Deckers, W. Desmet, Int. J. Solids Struct. **135**, 26 (2018).

*Corresponding author: qili@dlmu.edu.cn